ADVANCES IN ATMOSPHERIC SCIENCES
大气科学进展

EARLY ONLINE RELEASE

The DOI for this manuscript is doi: 10.1007/s00376-018-8022-9.

Nocturnal Low-level Winds and Their Impacts on Particulate Matter over the Beijing Area

Yong CHEN[1], Junling AN[*1,2,4], Yele SUN[1,2], Xiquan WANG[1], Yu QU[1], Jingwei ZHANG[1,2], Zifa WANG[1,2], and Jing DUAN[3]

[1]*State Key Laboratory of Atmospheric Boundary Layer Physics and Atmospheric Chemistry, Institute of Atmospheric Physics, Chinese Academy of Sciences, Beijing* 100029, *China*

[2]*College of Earth Science, University of the Chinese Academy of Sciences, Beijing* 100049, *China*

[3]*Chinese Academy of Meteorological Sciences, Beijing* 100081, *China*

[4]*Center for Excellence in Regional Atmospheric Environment, Institute of Urban Environment, Chinese Academy of Sciences, Xiamen* 361021, *China*

(Received 23 January 2018; revised 7 June 2018; accepted 20 June 2018)

ABSTRACT

Three-month wind profiles, 260 m PM_1 concentrations [i.e., particulate matter (PM) with an aerodynamic diameter ≤ 1 μm], and carrier-to-noise ratio data at two Beijing sites 55 km apart (urban and suburban) were collected to analyze the characteristics of low-level nocturnal wind and PM in autumn and winter. Three mountain-plain wind events with wind shear were selected for analysis. The measurements indicated that the maximum wind speeds of the northerly weak low-level jet (LLJ) below 320 m at the suburban site were weaker than

*Corresponding author: Junling AN
Email: anjl@mail.iap.ac.cn

those at the urban site, and the LLJ heights and depths at the suburban site were lower than those at the urban site. The nocturnal 140 m mean vertical velocities and the variations in vertical velocity at the urban site were larger than those at the suburban site. A nocturnal breeze with a weak LLJ of ~3 m s^{-1} noticeably offset nocturnal PM transport due to southerly flow and convergence within the northern urban area of Beijing. Characteristics of the nocturnal LLJ, such as start-up time, structure, intensity, and duration, were important factors in determining the decrease in the nocturnal horizontal range and site-based low-level variations in PM.

Key words: weak low-level jet, wind direction shear, wind lidar, low-level PM_1

1. Introduction

Most urban areas are located in complex geographical regions (e.g., mountains, coasts and lakes), and thus the spatial distribution of low-level winds in these areas could be influenced by dynamic effects of mountains (Hu et al., 2014) and thermally driven circulation modes by the different heating conditions, such as mountain-plain breezes, sea/lake breezes and urban heat island (UHI) circulation (Fernando et al., 2013; Leo et al., 2015; Hu and Xue, 2016; Dou and Miao, 2017; Zhang et al., 2017). Mountain-plain breezes are characterized by a reversal of wind direction twice per day, produced by atmospheric heating during daytime and cooling at nighttime. Because the concentration and distribution of air pollutants can be impacted by low-level wind patterns (Hu et al., 2014; Miao et al., 2015), knowledge of the

3D distributions of air pollutants and wind is very important for the interpretation of air pollution in urban areas (Baumbach and Vogt, 1999).

The air quality in urban areas with complex topography is largely modulated by thermally driven circulations under weak synoptic forcing. Urban ozone and particulate matter (PM) concentrations can be elevated by inland advection caused by sea/lake breezes during the daytime (Ding et al., 2004; Ji et al., 2013; Blaylock et al., 2017; Miao et al., 2017a; Zhang et al., 2017). Urban PM can be modulated by downslope winds and mountain-plain winds (Lee et al., 2003; Pardyjak et al., 2009; Fernando et al., 2013; Miao et al., 2015).

Beijing is located on the North China Plain, with the Yanshan and Taihang mountains to the north and west. As the capital of China and one of the largest megacities in the world, Beijing has been experiencing air pollution in recent years (Wang et al., 2014; Ye et al., 2016), resulting in considerable scientific attention focused on this city's air pollution patterns and underlying mechanisms, including the horizontal and vertical distribution of PM (Sun et al., 2010, Dong et al., 2013), the source of PM (Sun et al., 2016), and the relationship between PM and boundary layer height (BLH; Miao et al., 2015, 2017b; Tang et al., 2016; Huang et al., 2017; Zhu et al., 2018). The importance of local thermally driven circulations for air quality in the Beijing area has also been summarized by researchers (Wang et al., 2006; Chen et al., 2009; Miao et al., 2017a). Breezes that flow from the plains to the mountains can transport urban plumes to the mountainous areas around Beijing during the day, thereby increasing ozone concentrations (Wang et al., 2006). Elevated pollution layers over Beijing can form in summer due to the mountain chimney effect (Chen et al., 2009). Sea-breeze

fronts have been found to penetrate approximately 150 km inland during daytime, causing Bohai aerosols to be transported to Beijing (Miao et al., 2017a). However, previous studies have primarily focused on relatively strong thermally driven circulations in summer.

Nocturnal low-level jets (LLJs), streams of fast-moving air with the largest wind speeds in the lowest kilometers of the troposphere, can modulate the transport of heat and air pollutants along the surface due to the strong shear below each jet (Banta, 2008; Du et al., 2014; Wei et al., 2014; Klein et al., 2016; Miao et al., 2018). Nocturnal LLJs can increase surface ozone concentrations through horizontal advection and vertical mixing (Lee et al., 2003; Hu et al., 2013). Measurement of the nocturnal low-level wind profile in urban and suburban areas can be accomplished using a tethered balloon, a meteorological tower, or wind lidar (Wang et al., 2007; Li and Shu, 2008; Li et al., 2016; Jin et al., 2016). The height of the LLJ over urban areas has been shown to be higher than that over suburban areas in both plain and mountainous cities (Wang et al., 2007; Li and Shu, 2008). In addition, the diurnal trends, sources and formation mechanisms of low-level (< 300 m) PM concentrations have also been studied using tower data (Sun et al., 2010, 2016). However, few studies have focused on the characteristics of low-level nocturnal winds and PM at both urban and suburban sites.

Vertical wind shear, including directional shear and speed shear, can have important effects on pollutant transport (Bowen et al., 2000). In five events characterized by directional shear in Beijing, low-level PM increased during an evening transition period and then decreased gradually throughout the night (Chen et al., 2017c). Clear low-level wind shear and

zero horizontal wind zones with a delay of 1.5 h were found at two urban sites 20 km apart in Beijing (Chen et al., 2017b). However, such low-level wind and PM measurements taken simultaneously at both urban and suburban areas in Beijing are limited. Wind lidar has the ability to measure wind profiles and characterize the low-level variability of PM concentrations (Chen et al., 2017c). Therefore, the characteristics of nocturnal low-level wind and PM, as well as the impact of wind shear on PM over mountainous cities (e.g., Beijing), were obtained here using wind lidar deployed over the suburban/piedmont areas of Beijing, tower measurements of PM at 260 m, and a wind profile of the urban/plain areas of Beijing. The relationship between 10-m height wind and ground $PM_{2.5}$ (aerodynamic diameter ≤ 2.5 μm) was also analyzed, to discuss the impact of mountain breezes on the PM distribution. Our analysis focused on autumn and winter, when weak thermally driven circulations and pollution events occur more frequently in Beijing.

This paper is arranged as follows: Section 2 provides an overview of the study's sites, instrumentation, and measurements in the urban and suburban areas of Beijing. Section 3 describes the characteristics of nighttime low-level wind and PM at the study sites, based on three events selected from a dataset around three months in length, and discusses the impact of mountain breezes on PM. Concluding remarks are given in section 4.

2. Sites, instrumentation and measurements

2.1 *Sites*

The urban site [39°58´N, 116°22´E; 49 m ASL (above sea level)] selected for this study was located at the tower branch of the Institute of Atmospheric Physics, Chinese Academy of Sciences, between the third and fourth north ring road in Beijing (labeled “Tower” in Fig. 1a). The suburban site (40°24´N, 116°40´E; 90 m ASL) was located at the Yanqihu campus of the University of Chinese Academy of Sciences (labeled “Yanqihu” in Fig. 1a).

The straight-line distance between the two test sites is approximately 55 km. According to a study on the main urban area of Beijing (Jacobson et al., 2015), the sixth north ring road of Beijing can be considered the approximate northern boundary of the urban area. The straight-line distance between the tower site and the northern urban boundary is approximately 23 km when the straight-line path is between the tower and the site at Yanqihu. The urban site is located on a plain roughly 20--40 km away from the western and northern mountains. The site is surrounded by buildings with varying heights (20--90 m), which are used for residential, commercial and recreational purposes within a radius of approximately 1 km of the tower site (Al-Jiboori and Hu, 2005). The northern and northwestern areas of the suburban site are close enough to the foot of the Yanshan Mountains (Figs. 1a and b) that drainage winds can impact the site quickly after sunset.

2.2 *Instrumentation and measurements*

2.2.1 *Meteorological tower*

The 325-m meteorological tower at the urban site measures wind speed and direction (010C cup anemometers and 020C wind vanes, Metone, USA), and air temperature and

humidity (HC2-S3, Rotronic, Switzerland) at 15 levels: 8, 15, 32, 47, 65, 80, 100, 120, 140, 160, 180, 200, 240, 280 and 320 m AGL (above ground level). The cup anemometers are placed on two 4-m arms extending northwest and southeast from the cantilevers; the wind vanes are present only on the southeast cantilever. These wind sensors sample wind speed and direction at 0.05 Hz and a resolution of 0.1 m s^{-1} and 0.1°, and are useful when a low starting threshold (0.22 m s^{-1}) is required.

The three sets (47, 140 and 280 m) of turbulence instruments, each located on a cantilever pointing north from the tower, include 3D sonic anemometers (Windmaster Pro, Gill, UK), which measure wind velocity at a frequency of 10 Hz and a resolution of 0.01 m s^{-1} and 0.1°.

An aerosol chemical speciation monitor (ACSM, Aerodyne, USA) is deployed at 260 m on the 325-m tower to measure 5-min PM_1 mass concentrations (Chen et al., 2015; Sun et al., 2016). Mass concentrations of particulate organics, sulfate, nitrate, ammonium, and chloride are measured by the ACSM with a detection limit of < 0.2 μg m^{-3} for 30 min, which is suitable for measuring typical urban aerosol loadings (Ng et al., 2011). The PM_1 concentrations determined using the ACSM agree well with the $PM_{2.5}$ levels measured by a co-located (~30 m away) tapered element oscillating microbalance (Sun et al., 2012).

2.2.2 *Doppler wind lidar*

2.2.2.1 WindCube

A Doppler wind lidar, WindCube v1 (referred to as WLS8; Leosphere, France) was deployed on the roof of an educational building (~20 m AGL) at the Yanqihu site (Fig. 1c). Based on the velocity azimuthal display method, which computes the radial wind speed measurements along four cardinal directions separated by 90°, 10-level wind profiles from 40 m to 320 m (40, 80, 110, 140, 170, 200, 220, 240, 280 and 320 m) were measured using WLS8. The instrument produces a time series at each height with an average time of 1.1 s (using one new beam and three relatively old beams), an independent sampling rate of 4 s (using four new beams), and a resolution of 0.2 m s^{-1} and 1.5°. The maximum measured height and uncertainty depended on environmental and weather conditions, such as aerosol backscatter, turbulence, humidity, and precipitation (Aitken et al., 2012). Additional operating parameters of WLS8 can be found in Chen et al. (2017c).

2.2.2.2 Evaluation of WLS8-measured horizontal wind and estimated PM_1 trend

The horizontal wind speed and direction were measured by WLS8 over six months (from 18 October 2013 to 22 April 2014) and compared with those measured by wind cup anemometers mounted on the co-located 325-m tower. Both 10-min averaged wind speeds and direction were highly correlated (R = 0.96--0.99) at three levels (80, 140, and 200 m) (Chen et al., 2017c).

The carrier-to-noise ratio (CNRs) of a lidar are expected to be influenced by aerosol backscatter, atmospheric refractive turbulence, and so on. During weak turbulence and dry conditions, the CNRs of a lidar are highly correlated to particulate concentrations in the lowest part of the atmospheric boundary layer (Aitken et al., 2012). The variability and trend

in low-level (260 m) PM_1 concentrations were captured by the CNR of the WLS8 in a fair-weather period without long-range dust transport from co-located comparison between WLS8 and ACSM (Chen et al., 2017c).

2.2.2.3 Evaluation of mean vertical velocities measured by the WLS8

Co-located measurements were taken using the WLS8 and sonic anemometers at the tower site from 1 October 2014 to 20 October 2014. The relative distance and height of the WLS8 and tower were 50 m and 6 m, respectively. Two vertical velocity levels measured by the WLS8 and sonic anemometer (47 m and 140 m, respectively) were used.

According to the studies of Huang et al. (2017) and Chen et al. (2017a), vertical velocities measured by wind lidar agree well with sonic anemometer data only under low horizontal wind conditions. In addition, turbulence was overestimated because the Leosphere WindCube uses the last four cardinal direction measurements to project radial wind speeds (Kumer et al., 2016). To avoid these overestimations, the data of independent wind vectors based on every fourth measurement (Kumer et al., 2016) were use in this study.

Figure 2a shows a time series (24 h) of 10-min average vertical velocities measured by the WLS8 and sonic anemometer at 140 m AGL on 9 October 2014. Both 140-m vertical velocity measurements agree well under low 140-m horizontal wind speed conditions (< ~4 m s^{-1}). The 140-m correlation coefficient between the WLS8 and sonic anemometer under low horizontal wind conditions (< 3 m s^{-1}) is shown in Fig. 2b. The 140-m correlation coefficient between the WLS8 and sonic anemometer was 0.72 based on the measurements taken from 1 October 2014 to 20 October 2014, similar to the value (0.77) identified in Chen

et al. (2017a). The 140-m WLS8 measurements of vertical velocity were slightly higher than those taken by the sonic anemometer. The agreement between the WLS8 and sonic anemometer measurements was less at 47 m than that at 140 m AGL because 47 m falls within the roughness sublayer, and 140 m falls within the constant-flux layer (Miao et al., 2012). In other words, the average vertical velocities measured by the WLS8 and the sonic anemometer were comparable at 140 m AGL under low wind speed conditions.

The smaller correlation coefficient between the WLS8 and sonic anemometer data under strong wind conditions (Chen et al., 2017a) may be partly caused by an error arising from the vertical misalignment of the anemometer (Cheng et al., 2015), as well as different sampling volumes and measuring principles (Chintawongvanich et al., 1989).

2.2.3 *Other observational data*

Hourly ground $PM_{2.5}$ measurements from 35 stations within the Beijing Municipal Environmental Monitoring Center (http://zx.bjmemc.com.cn) were used in this study. Two surface $PM_{2.5}$ environmental sites, Huairou and the Olympic Center, which are close to Yanqihu and the tower sites (with distances of 10.0 km and 2.3 km, respectively), were also selected, to characterize the trend in ground $PM_{2.5}$ measurements at night (Fig. 1a).

Hourly 10-m wind from the dense network of automatic weather stations around Beijing (China Meteorological Administration) was used to determine the surface wind pattern in this study. The twice-daily radiosondes measurements (http://www.esrl.noaa.gov/raobs) of potential temperature and wind velocity profiles at Nanjiao station (labeled “Nanjiao” in Fig.

1a) were also used, to describe the depth of the vertical extension of mountain breezes. Nanjiao station is approximately 20 km from the tower site.

2.2.4 *Observational period and data processing*

Urban and suburban wind profile observations were conducted from 22 October 2014 to 18 January 2015, which covered the autumn and winter months in Beijing. Considering that WLS8 is located at ~20 m AGL, 20 m was added to the raw output of WLS8 for heights between 40 and 320 m. All data are reported in local standard time (LST, UTC+8).

3. Results and discussion

3.1 *Overview*

3.1.1 *Wind rose and diurnal cycle of low-level wind at both sites*

A wind rose measured at the lowest height (60 m AGL) using the WLS8 from the Yanqihu site was used to compare 65-m data from the tower site to understand the mean wind characteristics at both sites (Fig. 3). The patterns for the highest and lowest wind directions at both sites were similar. Both sites showed strong winds (> 7 m s^{-1}) originating primarily from the northwest and west. Two differences in low-level winds at each site were found: (1) calm wind frequencies (< 1 m s^{-1}) at the urban site were lower than those at the suburban site, with values of 12% and 30%, respectively; and (2) more westerly flows were measured at the urban site than at the suburban site as the wind became stronger. This observation could be explained by differences in topography and surrounding environments, which led to turbulent

orographic drag and blocking effects that were more obvious at the suburban site than at the urban site (Fig. 1b).

The diurnal cycle of low-level winds at the two sites based on three months of data is shown in Fig. 4. Wind speeds at the urban site were higher than those at the suburban site. Wind speeds at both the urban and suburban sites increased from around 0800 to 1500 LST during the daytime. After sunset, the suburban site exhibited a pulse in wind speed at 2000 LST, while the urban site exhibited a pulse at 2100 LST. To obtain information about local thermal circulation, only wind speeds lower than 3 m s^{-1} were calculated. Shifts in wind direction at both sites exhibited a reversal in direction twice per day. After sunset, a wind shift occurred at the suburban site, with a westerly wind apparent at 1700 LST, while a similar shift occurred at the urban site at 2300 LST. The highest speeds of the nocturnal northerly winds at the urban site were approximately 0200--0600 LST.

3.1.2 *Three events with vertical wind shear*

Wind shear has important effects on pollutant transport (Bowen et al., 2000). Wind shear caused by the mountain-plain winds around Beijing occurs on 17%--30% of days in autumn (Chen et al., 2017c). Thus, understanding the characteristics of frequently occurring wind shear events in Beijing can help us to better understand nocturnal breezes in Beijing and their impact on PM.

Three mountain-plain wind events featuring directional shear between two adjacent vertical layers during the day-to-night transition are shown in Table 1. The events---on 23, 24 and 28 October 2014---featured diurnal mountain-plain winds at both the urban and suburban

sites. Comparisons among the nocturnal low-level winds, PM variations, LLJ depths and heights, start times of directional shear shift and the LLJ were performed.

During these events, the Beijing area was controlled by weak synoptic forcing. Beijing was located west of a high pressure during these events, while Beijing was closer to the center of the high pressure on 28 October 2014, based on their sea level pressure field at 2000 LST and 0800 LST of the following day ［Fig. S1 in the Electronic Supplementary Material (ESM)］. The synoptic 10-m winds were southerly in Beijing under these conditions (Fig. S1).

To determine the temperature and wind characteristics at higher altitudes (> 300 m AGL) in the Beijing area during these events, their vertical temperature and wind profiles were measured using radiosondes (from Nanjiao station at 2000 and 0800 LST of the following day), the results of which are plotted in Fig. 5. Two temperature inversion layers, at < 200 m and approximately 600--1500 m AGL, were found at 2000 LST for these three events; and after one night, the intensity of temperature inversion between approximately 600 and 1000 m on 23 and 24 October became stronger. At 0800 LST, the wind speed of these three events was less than 5 m s^{-1} below 700 m AGL; and the events on 24, 28 October 2014 exhibited a nose at approximately 100--300 m. A change from southerly winds at 2000 LST to northerly winds at 0800 LST at 200--600 m AGL was found for these events, while southerly winds continued above 600 m AGL. This result suggests that mountain-plain winds can reach 600 m AGL in the southern Beijing area.

3.2. *Characteristics of nocturnal low-level mountain breezes*

3.2.1 *Wind shift and weak LLJ*

Figure 6 presents the horizontal wind profiles, CNRs, and PM_1 mass concentrations observed at the Yanqihu and tower sites on 28 October 2014. At the Yanqihu site, a northerly wind component at 60 m indicated the occurrence of a local downslope flow after sunset and through the night (Fig. 6a), while the start time of 47-m day-to-night wind shifts at the tower site was 2200 LST (Fig. 6b). The start times of day-to-night wind shifts for the 23 and 24 October events are also listed in Table 1. Variations in the day-to-night wind direction on 23, 24 and 28 October at the Yanqihu and tower sites exhibited southerly-to-northwesterly and southerly-to-northerly flows, respectively (Table 1). In addition, for the 28 October event, the wind shift from southerly to northerly below 340 m lasted around 4 h at both sites (Fig. 6); furthermore, the wind speeds during the transition period exhibited wind shears of 1--2 m s^{-1} at both sites (Fig. 6) and were associated with minimal wind speed at certain heights. Similar wind shifts on 23 and 24 October are shown in Figs. S2 and S3.

The definition of an LLJ varies among studies depending on their application; maximum wind speeds at levels both above and below the jet nose may be required (Banta, 2008). Because a weak jet-like structured wind profile can impact pollutant transport (Banta et al., 2007), and generated turbulence can affect surface fluxes (Banta, 2008), it is important to know the properties of the weak jet-like wind profile and understand its impacts on pollutant transport. Banta et al. (2002) used objective criteria to define a weak LLJ based on 0.5 m s^{-1} decreases above and below the jet nose using high-resolution lidar. We also used this definition of a weak LLJ (Banta et al., 2002) in this study.

To obtain the average characteristics of a weak LLJ, we depicted mean and maximum horizontal wind speeds (10-min data) during 2300--0700 LST for three events, which are shown in Fig. 7. Maximum wind speeds of the LLJ below 320 m at the Yanqihu site were lower than those at the tower site (2--4 m s^{-1} vs. 3--5 m s^{-1}; Fig. 7). The heights and depths of the LLJ core at the Yanqihu site were also lower than those at the tower site (Figs. 7 and S4). The start time of the LLJ for two events (23 and 24 October) at the Yanqihu site was 3--5 h later than that at the tower site, although the start time for one event (28 October) was 3 h earlier at the Yanqihu site than that at the tower site (Table 1).

The mean nocturnal LLJ height at the urban site for the three events was 150--200 m. The LLJ height at an urban site (Beiwalu) located approximately 7 km southwest of the tower site was 200--240 m, which was higher than the 100--140 m height at two suburban sites (Xisanqi and Nanjiao) observed in summer 2004 by tethered balloon (Li and Shu, 2008). The LLJ height at the urban site in the present study was in agreement with that in the study by Li and Shu (2008) in summer. The slightly lower LLJ height may be caused by (1) the relatively weak strength of the mountain-plain winds in autumn and winter, and (2) their different nocturnal BLH (Klein et al., 2016). The summer jet height at the urban site was higher than that at the suburban site, which was also observed by Wang et al. (2007) and Li and Shu (2008). The wind speed of the LLJ in the urban area was stronger than that upstream of the suburban area—a result that is similar to the observation in Beijing by Li and Shu (2008), but different from the observation in Oklahoma City by Wang et al. (2007), who showed that the wind speed of the LLJ in their urban area was 10%--15% slower than that in their suburban

area. However, the urban and suburban/rural study areas in Wang et al. (2007) were only 6 km apart, representing a smaller scale by comparison with the megacity of Beijing. Additionally, the convergence of the mountain-plain winds in urban Beijing may be stronger than that in the northern suburban area, while Oklahoma City does not experience mountain-plain winds.

3.2.2 *Mean vertical velocities*

In a relatively flat area, vertical velocities are generally weak (< 1 cm s^{-1}) in the stable boundary layer and may not be important in the vertical transport of pollutants (Fast and Darby, 2004). However, areas with complex topographies are likely to produce strong vertical motion due to convergence and divergence (Fast and Darby, 2004). The observed low-level (140--160 m AGL) mean vertical velocities of the three events in October at the urban and suburban sites are shown in Fig. 8. The observed heights of the mean vertical velocities are located in the bottom or middle of the LLJ.

Stronger descending motion was observed at the urban site than at the suburban site after sunset, while ascending motion occurred after 2100--2200 LST and 1900 LST at the urban and suburban sites, respectively (Fig. 8). The mean vertical velocity during 2200--0700 LST at the urban site was 5.6--6.7 cm s^{-1}, which was greater than that at the suburban site, where values of only 1.3--4.7 cm s^{-1} were observed (Table 2). The variance in vertical velocity at the urban site during 2200--0700 LST was also higher than that at the suburban site, except for the 23 October event (Table 2). These differences between urban and suburban areas may be attributable to different convergence zones and thermal environments. Warmer

temperatures at the urban site caused by the UHI effect (Dou and Miao, 2017) lead to a stronger updraft.

The 140-m mean vertical velocity at the urban site during the LLJ period was weaker than that during the previous LLJ period, which experienced a northerly wind shift on 23 and 24 October (~4--6 cm s^{-1} vs. ~8 cm s^{-1}, respectively); the results from both of these events are comparable with the result from the 28 October event (within ~6 cm s^{-1}) (Fig. 8). It is noted that the LLJ occasionally had intermittent downdrafts, which lowered the mean vertical velocity. During the LLJ period, the weakest 140-m horizontal wind speed on 28 October caused the weakest downdraft and the strongest mean vertical velocity (Fig. 8). These horizontal wind speeds can also be explained by their relative locations (i.e., bottom or middle) within the measured altitude (140 m AGL) compared to the LLJ core. In other words, the mean vertical velocity over the urban site during the LLJ period was weaker than that during the previous LLJ period, which occurred in the middle of the LLJ; however, the mean vertical velocity over the urban site was comparable with that at the bottom of the LLJ region.

3.3 *Impact of mountain breezes on PM*

3.3.1 *Low-level and surface variations in PM and CNR at both sites*

The patterns in PM_1 and CNR variations during the day-to-night transition and at night at both sites are presented in the lower portions of Figs. 6 and S2--S3, and are summarized in Table 1. The 260-m PM_1 concentrations and CNRs for the three events at both sites first

increased then decreased during the day-to-night transition and at night, except for the Yanqihu site on 28 October. Note that the low-level CNR and PM at the suburban site increased until 0500 LST on 23 and 24 October, while those at the urban site exhibited a delay of around 1--2 h once the northerly wind arrived (Figs. S2 and S3).

The urban site surface variations in $PM_{2.5}$ for the three events in October at the Olympic Center site were almost synchronous with the 260-m urban measurements at a distance of 2.3 km (Figs. 9, 6, S2 and S3). However, the suburban (Huairou; 10 km away from Yanqihu) surface $PM_{2.5}$ trends on 23 and 24 October events differed from the low-level CNR (60 and 260 m AGL) at the Yanqihu site, where surface $PM_{2.5}$ decreased during 2000--2300 LST, and low-level $PM_{2.5}$ decreased until at 0500 LST (Figs. 9, 6, S2 and S3). This pattern suggests that there could be different vertical PM profiles between the Yanqihu site and the tower site, based on their different $PM_{2.5}$ trends at the surface and at low-level heights.

Fernando et al. (2013) found a PM increase at the surface at two sites in Phoenix during the transition period and noted that this increase could be caused by entrainment from the transition front, which leads to subsequent turbulent mixing. Chen et al. (2017c) also found a PM increase at 80 and 200 m AGL during the transition period in urban Beijing. We conducted an observational study of low-level PM concentrations during the transition period at two sites (urban and suburban Beijing) and found PM increases. This can be explained by horizontal advection that led to the return of aerosols, which were previously transported toward the foot of the mountains during the daytime (Ren et al., 2004), and wind shear, which induced vertical mixing (Fernando et al., 2013). The observed decrease in PM after the

transition period at the urban site was primarily caused by the arrival and persistence of the northerly weak LLJ (Figs. 6b, S2b and S3b). Low-level PM variations after the transition period at the suburban site were complex; the two events on 23 and 24 October showed a decreasing PM trend that accompanied an LLJ similar to that at the urban site, while the PM on 28 October remained roughly the same and then increased (Figs. 6a and S2a and S3a). The different intensities, structures and durations of the LLJ, which at the urban site exhibited a more closed core at 260 m with stronger wind speeds and longer durations, could be one of the important reasons for the different relationships between low-level PM and LLJs at the urban and suburban sites.

3.3.2 *Effect of surface wind convergence on surface PM distribution*

The horizontal distributions of surface $PM_{2.5}$ concentrations were also used to determine the impact of mountain-plain winds on PM distributions. In this section, we focus on the effect of surface wind convergence on the surface $PM_{2.5}$ distribution.

Nocturnal LLJs at the tower site were observed from around 2000--0100 LST (Table 1). The horizontal 10-min wind of the 28 October event, which showed the weakest mean low-level wind speed of the three events at the tower site, was analyzed in detail to determine the effect of surface wind convergence on the surface $PM_{2.5}$ distribution. Figure 10e shows the horizontal distribution of 10-m wind at 2300 LST on 28 October and suggests that the mountain-plain breeze assisted by northerly and northwesterly winds had already reached the 4th ring road of Beijing by that time. The urban core was engulfed by northerly winds at 0200

LST on 29 October (Fig 10f). However, an LLJ occurred at approximately 0400--0700 LST over the urban area, according to the tower wind profile (Fig. 6b).

Using the surface $PM_{2.5}$ concentration at 0200 LST as a reference, surface $PM_{2.5}$ concentrations at most urban stations decreased by more than 20% at 0700 LST during three events (Fig. 10 a and b); on 28 October, the southern urban sites exhibited increases of ~20%, while the northern urban sites exhibited decreases (Fig. 10c). However, when using the surface $PM_{2.5}$ concentration at 0500 LST as a reference, $PM_{2.5}$ concentrations in the urban core of Beijing decreased by almost 20% due to the arrival of the LLJ at 0500--0700 LST, while that in other areas of Beijing decreased by less than 10% (Fig. 10d). These 0200 and 0700 LST wind and $PM_{2.5}$ patterns imply that a mountain-plain wind with weak LLJ wind speeds of approximately 3 m s^{-1} could noticeably offset nocturnal pollutant transport due to southerly flow and convergence (at least in northern Beijing). The start-up time, intensity and duration of the LLJ caused by the nocturnal mountain breeze were likely important factors in determining the decrease in the nocturnal range of $PM_{2.5}$ over Beijing.

3.3.3 *Discussion of other effects on the PM trend and horizontal distribution*

The diurnal variations of BLH and pollutant emissions may also influence the diurnal and horizontal distribution of PM.

The BLH is one of the major factors affecting the diffusion of pollutants (Zhu et al., 2018). A relatively low BLH may cause a greater accumulation of pollutants under the same pollutant emission conditions. Schäfer et al. (2006) indicated that the BLH can account for more than 50% of the variation in the near-surface concentrations of pollutants, especially at

urban sites in winter. Zhu et al. (2018) used ceilometers to study the diurnal variation of BLH at the tower site in autumn (from December 2013 to November 2014). The nocturnal BLH at the tower site was less than 400 m, and a minor increase in the BLH with a growth rate less than approximately 10 m h^{-1} occurred from 0100 to 0700 LST (Zhu et al., 2018), suggesting the elevated BLH from 0100 to 0700 LST was also an important factor influencing the nocturnal $PM_{2.5}$ decrease.

The volume of emissions in Beijing related to power, industry, residential activity and vehicle use was almost at a minimum during 0000--0600 LST (Wang et al., 2010). However, black carbon in urban Beijing remained at high levels from the night to early next morning, because heavy-duty diesel vehicles (HDVs) are allowed to enter urban Beijing inside the 5th Ring Road from 0000 to 0600 LST (Song et al, 2013; Ji et al., 2018). The HDV emissions at around 0000 LST could be a factor in the increase of PM at the urban site at around 0000 LST.

4. Summary

Nocturnal low-level wind and PM characteristics at urban/plain (325-m tower) and suburban/piedmont (Yanqihu) sites in Beijing were studied using wind profiles, in-situ PM_1 mass concentrations, and CNRs observed by a 325 m tower and wind lidar. The datasets at both sites spanned three months in 2014 during autumn and winter. Three mountain-plain wind events characterized by vertical wind shear at both the urban and suburban sites were selected for analysis. Figure 11 illustrates the nocturnal mountain breeze schematics and their

impacts on PM over Beijing at both the suburban and urban sites, based on our observations. The main findings can be summarized as follows:

(1) The suburban site was mainly impacted by downslope winds, while the urban site was impacted by the convergence of mountain-plain winds and UHI circulation. The calm wind frequencies (< 1 m s^{-1}) at the urban site (12%) were lower than those at the suburban site (30%), based on the three months of data. The radiosonde measurements suggest that the height of the mountain-plain winds could reach 600 m AGL in southern Beijing.

(2) Day-to-night wind shifts of approximately 60 m occurred at around 2200 LST at the urban site and at around 1700 LST at the suburban site. The wind speeds, core heights and depths of the nocturnal LLJ below 320 m were lower at the suburban site than at the urban site. The mean vertical velocity and variance in vertical velocity at 140--160 m AGL during 2200--0700 LST at the urban site were higher than those at the suburban site.

(3) The 260-m PM_1/CNR data for most events at both sites first increased and then decreased during and after the evening transition period. The PM increase observed during the transition period could have been caused by horizontal advection that led to the return of aerosols, which were previously transported over the foot of the mountains in the daytime, and wind shear induced the vertical mixing of aerosols. The decrease in PM observed after the transition period could have been caused by the LLJ removal effect of aerosols.

(4) Mountain-plain breezes, which exhibited a weak LLJ of approximately 3 m s^{-1}, noticeably offset nocturnal $PM_{2.5}$ transport due to southerly flow and convergence, at least within the northern urban area of Beijing.

(5) The start-up time, structure, intensity, and duration of the weak LLJ caused by the nocturnal mountain breeze were important factors in determining the decrease in nocturnal horizontal range and site-based low-level variations in $PM_{2.5}$.

This study provides an improved understanding of nocturnal mountain breeze characteristics and their impact on PM distributions. However, the results still suffer from limitations due to location, environment, and equipment differences between the two sites. Further comprehensive observations of PM, BLH and meteorological vertical profiles (i.e., wind and temperature) at additional sites and more detailed numerical simulations by a mesoscale meteorological/aerosol model are still needed to represent the detailed 3D distributions of winds and PM concentrations to obtain the quantitative effect of nocturnal mountain breezes on aerosols.

Acknowledgments. We are sincerely thankful to senior engineer Aiguo LI from the Institute of Atmospheric Physics, Chinese Academy of Sciences, for providing the data of the 325-m Beijing meteorological tower. This work was supported by the National Key R&D Program of China (Grant No. 2017YFC0209801) and the National Natural Science Foundation of China (Grant Nos. 41505091, 91544221, 41675137, 41575124 and 41505116). We would also like to thank the anonymous reviewers and editors for their key suggestions that helped improve the original manuscript.

Electronic supplementary material: Supplementary material is available in the online version of this article at https://doi.org/10.1007/s00376-018-8022-9.

REFERENCES

Aitken, M. L., M. E. Rhodes, and J. K. Lundquist, 2012: Performance of a wind-profiling lidar in the region of wind turbine rotor disks. *J. Atmos. Ocean. Technol.*, **29**, 347--355, https://doi:10.1175/JTECH-D-11-00033.1.

Al-Jiboori, M. H., and F. Hu, 2005: Surface roughness around a 325-m meteorological tower and its effect on urban turbulence. *Adv. Atmos. Sci.*, **22**, 595--605, https://doi.org/10.1007/BF02918491.

Banta, R. M., 2008: Stable-boundary-layer regimes from the perspective of the low-level jet. *Acta Geophysica*, **56**, 58--87, https://doi.org/10.2478/s11600-007-0049-8.

Banta, R. M., R. K. Newsom, J. K. Lundquist, Y. L. Pichugina, R. L. Coulter, and L. Mahrt, 2002: Nocturnal low-level jet characteristics over Kansas during CASES-99. *Bound.-Layer Meteor.*, **105**, 221--252, https://doi.org/10.1023/A:1019992330866.

Banta, R. M., L. Mahrt, D. Vickers, J. L. Sun, B. B. Balsley, Y. L. Pichugina, and E. J. Williams, 2007: The very stable boundary layer on nights with weak low-level jets. *J. Atmos. Sci.*, **64**, 3068--3090, https://doi.org/10.1175/JAS4002.1.

Baumbach, G., and U. Vogt, 1999: Experimental determination of the effect of mountain-valley breeze circulation on air pollution in the vicinity of Freiburg. *Atmos. Environ.*, **33**, 4019--4027, https://doi.org/10.1016/S1352-2310(99)00143-0.

Blaylock, B. K., J. D. Horel, and E. T. Crosman, 2017: Impact of lake breezes on summer ozone concentrations in the Salt Lake valley. *Journal of Applied Meteorology and Climatology*, **56**, 353--370, https://doi.org/10.1175/JAMC-D-16-0216.1.

Bowen, B. M., J. A. Baars, and G. L. Stone, 2000: Nocturnal wind direction shear and its potential impact on pollutant transport. *J. Appl. Meteor.*, **39**, 437--445, https://doi.org/10.1175/1520-0450(2000)039<0437:NWDSAI>2.0.CO;2.

Chen, C., and Coauthors, 2015: Characteristics and sources of submicron aerosols above the urban canopy (260 m) in Beijing, China, during the 2014 APEC summit. *Atmos. Chem. Phys.*, **15**, 12 879--12 895, https://doi.org/10.5194/acp-15-12879-2015.

Chen, W. C., L. L. Song, Z. C. Wang, and A. J. Liu, 2017a: The wind measuring performance of WINDCUBE V2 pulse laser wind profiler under different weather conditions. *Journal of Applied Meteorological Science*, **28**(3), 327—339, https://doi.org/10.11898/1001-7313.20170307. (in Chinese)

Chen, Y., C. S. Zhao, Q. Zhang, Z. Z. Deng, M. Y. Huang, and X. C. Ma, 2009: Aircraft study of Mountain Chimney effect of Beijing, China. *J. Geophys. Res.*, **114**, D08306, https://doi.org/10.1029/2008JD010610.

Chen, Y., J.-L. An, J. Lin, Y.-L. Sun, X.-Q. Wang, Z.-F. Wang, and J. Duan, 2017b: Observation of nocturnal low-level wind shear and particulate matter in urban Beijing using a Doppler wind lidar. *Atmos. Ocean. Sci. Lett.*, **10**(6), 411-417, https://doi.org/10.1080/16742834.2017.1368349.

Chen, Y., J. L. An, X. Q. Wang, Y. L. Sun, Z. F. Wang, and J. Duan, 2017c: Observation of wind shear during evening transition and an estimation of submicron aerosol concentrations in Beijing using a Doppler wind lidar. *Journal of Meteorological Research*, **31**, 350--362, https://doi.org/10.1007/s13351-017-6036-3.

Cheng, X. L., Z. Peng, F. Hu, Q. C. Zeng, W. D. Luo, Y. J. Zhao, and Z. X. Hong, 2015: Measurement errors and correction of the UAT-2 ultrasonic anemometer. *Science China Technological Sciences*, **58**, 677--686, https://doi.org/10.1007/s11431-014-5728-5.

Chintawongvanich, P., R. Olsen, and C. A. Biltoft, 1989: Intercomparison of wind measurements from two acoustic Doppler sodars, a laser Doppler lidar, and in situ sensors. *J. Atmos. Oceanic Technol.*, **6**, 785--797, https://doi.org/10.1175/1520-0426(1989)006<0785:IOWMFT>2.0.CO;2.

Ding, A. J., T. Wang, M. Zhao, T. J. Wang, and Z. K. Li, 2004: Simulation of sea-land breezes and a discussion of their implications on the transport of air pollution during a multi-day ozone episode in the Pearl River Delta of China. *Atmos. Environ.*, **38**, 6737--6750, https://doi.org/10.1016/j.atmosenv.2004.09.017.

Dong, F., X. Q. Wang, Z. F. Wang, P. Z. Yan, 2013: A study of the north-south differences of the air quality in Beijing. *Climatic and Environmental Research*, **18**, 63-70, https://doi.org/10.3878/j.issn.1006-9585.2012.11035. (in Chinese)

Dou, J. J., and S. G. Miao, 2017: Impact of mass human migration during Chinese New Year on Beijing urban heat island. *Int. J. Climatol*, **37**, 4199--4210, https://doi.org/10.1002/joc.5061.

Du, Y., Q. H. Zhang, Y. L. Chen, Y. Y. Zhao, and X. Wang, 2014: Numerical simulations of spatial distributions and diurnal variations of low-level jets in China during early summer. *J. Climate*, **27**, 5747--5767, https://doi.org/10.1175/JCLI-D-13-00571.1.

Fast, J. D., and L. S. Darby, 2004: An evaluation of mesoscale model predictions of down-valley and canyon flows and their consequences using Doppler lidar measurements during VTMX 2000. *J. Appl. Meteor.*, **43**, 420--436, https://doi.org/10.1175/1520-0450(2004)043<0420:AEOMMP>2.0.CO;2.

Fernando, H. J. S., B. Verhoef, S. Di Sabatino, L. S. Leo, and S. Park, 2013: The Phoenix Evening Transition Flow Experiment (TRANSFLEX). *Bound.-Layer Meteor.*, **147**, 443--468, https://doi.org/10.1007/s10546-012-9795-5.

Hu, X.-M., and M. Xue, 2016: Influence of synoptic sea-breeze fronts on the urban heat island intensity in Dallas-Fort Worth, Texas. *Mon. Wea. Rev.*, **144**, 1487--1507, https://doi.org/10.1175/MWR-D-15-0201.1.

Hu, X.-M., P. M. Klein, M. Xue, F. Q. Zhang, D. C. Doughty, R. Forkel, E. Joseph, and J. D. Fuentes, 2013: Impact of the vertical mixing induced by low-level jets on boundary layer ozone concentration. *Atmos. Environ.*, **70**, 123--130, https://doi.org/10.1016/j.atmosenv.2012.12.046.

Hu, X.-M., and Coauthors, 2014: Impact of the Loess Plateau on the atmospheric boundary layer structure and air quality in the North China Plain: A case study. *Science of the Total Environment* **499**, 228--237, https://doi.org/10.1016/j.scitotenv.2014.08.053.

Huang, M., Z. Q. Gao, S. G. Miao, F. Chen, M. A. LeMone, J. Li, F. Hu, and L. L. Wang, 2017: Estimate of boundary-layer depth over Beijing, China, using Doppler lidar data during SURF-2015. *Bound.-Layer Meteor.*, **162**, 503--522, https://doi.org/10.1007/s10546-016-0205-2.

Jacobson, M. Z., S. V Nghiem, A. Sorichetta, and N. Whitney, 2015: Ring of impact from the mega-urbanization of Beijing between 2000 and 2009. *J. Geophys. Res.*, **120**, 5740--5756, https://doi.org/10.1002/2014JD023008.

Ji, D. S., and Coauthors, 2018: Two-year continuous measurements of carbonaceous aerosols in urban Beijing, China: Temporal variations, characteristics and source analyses. *Chemosphere*, **200**, 191--200, https://doi.org/10.1016/j.chemosphere.2018.02.067.

Ji, H.-E., S.-H. Lee, and H.-W. Lee, 2013: Characteristics of sea breeze front development with various synoptic conditions and its impact on lower troposphere ozone formation. *Adv. Atmos. Sci.*, **30**, 1461--1478, https://doi.org/10.1007/s00376-013-2256-3.

Jin, L. L., Z. J. Li, Q. He, Q. L. Miao, H. Q. Zhang, and X. H. Yang, 2016: Observation and simulation of near-surface wind and its variation with topography in Urumqi, West China. *Journal of Meteorological Research*, **30**, 961--982, https://doi.org/10.1007/s13351-016-6012-3.

Klein, P. M., X.-M. Hu, A. Shapiro, and M. Xue, 2016: Linkages between boundary-layer structure and the development of nocturnal low-level jets in Central Oklahoma. *Bound.-Layer Meteor.*, **158**, 383--408, https://doi.org/10.1007/s10546-015-0097-6.

Kumer, V.-M., J. Reuder, M. Dorninger, R. Zauner, and V. Grubišić, 2016: Turbulent kinetic energy estimates from profiling wind LiDAR measurements and their potential for wind energy applications. *Renewable Energy*, **99**, 898--910, https://doi.org/10.1016/j.renene.2016.07.014.

Lee, S.-M., H. S. Fernando, M. Princevac, D. Zajic, M. Sinesi, J. L. McCulley, and J. Anderson, 2003: Transport and diffusion of ozone in the nocturnal and morning planetary boundary layer of the Phoenix valley. *Environmental Fluid Mechanics*, **3**, 331-362, https://doi.org/10.1023/A:1023680216173.

Leo, L. S., H. J. S. Fernando, and S. Di Sabatino, 2015: Near-surface flow in complex terrain with coastal and urban influence. *Environmental Fluid Mechanics*, **15**, 349--372, https://doi.org/10.1007/s10652-013-9327-y.

Li, J., and W.-J. Shu, 2008: Observation and analysis of nocturnal low-level jet characteristics over Beijing in summer. *Chinese Journal of Geophysics*, **51**, 360—368, https://doi.org/10.3321/j.issn:0001-5733.2008.02.008. (in Chinese)

Li, J., X.-Y. Cao, Z.-G. Cheng, J.-X. Dou, J.-J. Zhang, 2016: Analysis of spectral characteristics for wind velocity in the low layer of the atmosphere in the Beijing-Tianjin-Hebei city cluster area during summer. *Chinese Journal of Geophysics*, **59**, 1553—1565, https://doi.org/10.6038/cjg20160501. (in Chinese)

Miao, S. G., J. X. Dou, F. Chen, J. Li, and A. G. Li, 2012: Analysis of observations on the urban surface energy balance in Beijing. *Science China Earth Sciences*, **55**, 1881--1890, https://doi.org/10.1007/s11430-012-4411-6.

Miao, Y. C., X.-M. Hu, S. H. Liu, T. T. Qian, M. Xue, Y. J. Zheng, and S. Wang, 2015: Seasonal variation of local atmospheric circulations and boundary layer structure in the Beijing-Tianjin-Hebei region and implications for air quality. *Journal of Advances in Modeling Earth Systems*, **7**, 1602--1626, https://doi.org/10.1002/2015MS000522.

Miao, Y. C., J. P. Guo, S. H. Liu, H. Liu, G. Zhang, Y. Yan, and J. He, 2017a: Relay transport of aerosols to Beijing-Tianjin-Hebei region by multi-scale atmospheric circulations. *Atmos. Environ.*, **165**, 35--45, https://doi.org/10.1016/j.atmosenv.2017.06.032.

Miao, Y. C., J. P. Guo, S. H. Liu, H. Liu, Z. Q. Li, W. C. Zhang, and P. M. Zhai, 2017b: Classification of summertime synoptic patterns in Beijing and their associations with boundary layer structure affecting aerosol pollution. *Atmos. Chem. Phys.*, **17**, 3097--3110, https://doi.org/10.5194/acp-17-3097-2017.

Miao, Y. C., J. P. Guo, S. H. Liu, W. Wei, G. Zhang, Y. L. Lin, and P. M. Zhai, 2018: The climatology of low-level jet in Beijing and Guangzhou, China. *J. Geophys. Res*, **123**, 2816--2830, https://doi.org/10.1002/2017JD027321.

Ng, N. L., and Coauthors, 2011: An Aerosol Chemical Speciation Monitor (ACSM) for routine monitoring of the composition and mass concentrations of ambient aerosol. *Aerosol Science and Technology*, **45**, 780--794, https://doi.org/10.1080/02786826.2011.560211.

Pardyjak, E. R., H. J. S. Fernando, J. C. R. Hunt, A. A. Grachev, and J. Anderson, 2009: A case study of the development of nocturnal slope flows in a wide open valley and

associated air quality implications. *Meteor. Z.*, **18**, 85--100, https://doi.org/10.1127/0941-2948/2009/362.

Ren, Z. H., and Coauthors, 2004: Influence of weather system of different scales on pollution boundary layer and the transport in horizontal current field. *Research of Environmental Sciences*, **17**, 7--13, https://doi.org/10.3321/j.issn:1001-6929.2004.01.002. (in Chinese)

Schäfer, K., S. Emeis, H. Hoffmann, and C. Jahn, 2006: Influence of mixing layer height upon air pollution in urban and sub-urban areas. *Meteor. Z.*, **15**, 647--658, https://doi.org/10.1127/0941-2948/2006/0164.

Song, S. J., Y. Wu, J. Y. Xu, T. Ohara, S. Hasegawa, J. Q. Li, L. Yang, and J. M. Hao, 2013: Black carbon at a roadside site in Beijing: Temporal variations and relationships with carbon monoxide and particle number size distribution. *Atmos. Environ.*, **77**, 213--221, https://doi.org/10.1016/j.atmosenv.2013.04.055.

Sun, Y., Y. S. Wang, and C. C. Zhang, 2010: Vertical observations and analysis of $PM_{2.5}$, O_3, and NO_x at Beijing and Tianjin from towers during summer and autumn 2006. *Adv. Atmos. Sci.*, **27**, 123--136, https://doi.org/10.1007/s00376-009-8154-z.

Sun, Y. L., Z. F. Wang, H. B. Dong, T. Yang, J. Li, X. L. Pan, P. Chen, and J. T. Jayne, 2012: Characterization of summer organic and inorganic aerosols in Beijing, China with an Aerosol Chemical Speciation Monitor. *Atmos. Environ.*, **51**, 250--259, https://doi.org/10.1016/j.atmosenv.2012.01.013.

Sun, Y. L., and Coauthors, 2016: "APEC Blue": Secondary aerosol reductions from emission controls in Beijing. *Scientific Reports*, **6**, 20668, https://doi.org/10.1038/srep20668.

Tang, G. Q, and Coauthors, 2016: Mixing layer height and its implications for air pollution over Beijing, China. *Atmos. Chem. Phys.*, **16**, 2459--2475, https://doi.org/10.5194/acp-16-2459-2016.

Wang, T., A. J. Ding, J. Gao, and W. S. Wu, 2006: Strong ozone production in urban plumes from Beijing, China. *Geophys. Res. Lett.*, **33**, L21806, https://doi.org/10.1029/2006GL027689.

Wang, X. Y., and Coauthors, 2010: WRF-Chem simulation of East Asian air quality: Sensitivity to temporal and vertical emissions distributions. *Atmos. Environ.*, **44**, 660--669, https://doi.org/10.1016/j.atmosenv.2009.11.011.

Wang, Y. S., C. L. Klipp, D. M. Garvey, D. A. Ligon, C. C. Williamson, S. S. Chang, R. K. Newsom, and R. Calhoun, 2007: Nocturnal low-level-jet-dominated atmospheric boundary layer observed by a Doppler lidar over Oklahoma City during JU2003. *Journal of Applied Meteorology and Climatology*, **46**, 2098--2109, https://doi.org/10.1175/2006JAMC1283.1.

Wang, Y. S., and Coauthors, 2014: Mechanism for the formation of the January 2013 heavy haze pollution episode over central and eastern China. *Science China Earth Sciences*, **57**, 14--25, https://doi.org/10.1007/s11430-013-4773-4.

Wei, W., H. S. Zhang, and X. X. Ye, 2014: Comparison of low-level jets along the north coast of China in summer. *J. Geophys. Res.*, **119**, 9692--9706, https://doi.org/10.1002/2014JD021476.

Ye, X. X., Y. Song, X. H. Cai, and H. S. Zhang, 2016: Study on the synoptic flow patterns and boundary layer process of the severe haze events over the North China Plain in January 2013. *Atmos. Environ.*, **124**, 129--145, https://doi.org/10.1016/j.atmosenv.2015.06.011.

Zhang, L., B. Zhu, J. H. Gao, and H. Q. Kang, 2017: Impact of Taihu Lake on city ozone in the Yangtze River Delta. *Adv. Atmos. Sci.*, **34**, 226--234, https://doi.org/10.1007/s00376-016-6099-6.

Zhu, X. W., and Coauthors, 2018: Mixing layer height on the North China Plain and meteorological evidence of serious air pollution in southern Hebei. *Atmos. Chem. Phys.*, **18**, 4897--4910, https://doi.org/10.5194/acp-18-4897-2018.

Table 1. Characteristics of low-level winds and PM in suburban and urban Beijing.

Night	WD shift at 60 m/65 m AGL start time (LST)		WS jet start time (LST)		WD change		PM change	
	Suburban	Urban	Suburban	Urban	Suburban	Urban	Suburban	Urban
23 Oct 2014	1800	2200	0130	2230	S-NW	S-N	I-D	I-D
24 Oct 2014	1900	2030	0330	2130	S-NW	S-N	I-D	I-D
28 Oct 2014	1700	2230	2200	0100	S-NW	S-N	I	I-D

Notes: I, an increase in PM; I-D, an increase followed by a decrease in PM; WD, wind direction; WS, wind speed.

Table 2. Average 10-min vertical velocity (ω) values and 30-min variance in vertical velocity (σ_ω^2) at 140 m/160 m AGL in suburban and urban Beijing, respectively, during 2200--0700 LST.

Night	ω (m s^{-1})		σ_ω^2 (m^2 s^{-2})	
	Suburban	Urban	Suburban	Urban
23 Oct 2014	0.035	0.067	0.014	0.008
24 Oct 2014	0.047	0.056	0.008	0.031
28 Oct 2014	0.013	0.062	0.002	0.019

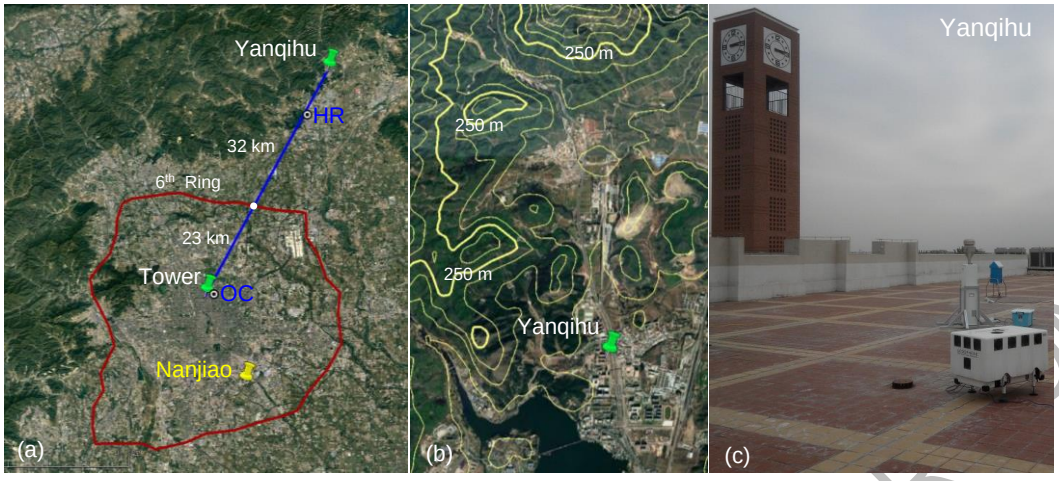

Fig. 1. (a) Locations of the 325-m meteorological tower (urban) site, the WLS8 at the Yanqihu (suburban) site, the Nanjiao sounding site, the Huairou (HR) and Olympic Center (OC) environmental stations, and the sixth ring road in Beijing. (b) High-resolution topography (50-m contour lines marked in yellow; bold yellow line represents 250 m ASL) of the Yanqihu site. (c) Photo of the WLS8 at the Yanqihu site. Note: maps derived from Google Earth.

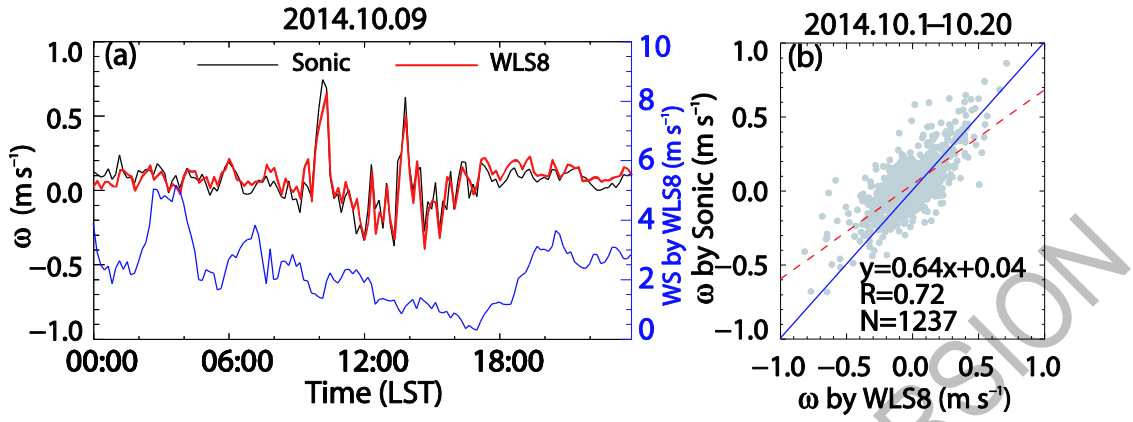

Fig. 2. (a) Comparison of the 10-min average vertical velocities measured by the WLS8 and the sonic anemometer at 140 m AGL at the urban site (tower) on 9 October 2014, and (b) during 1--20 October 2014 (excluding the rain and missing WLS8 data when the 140-m horizontal wind speed was less than 3 m s^{-1}). Notes: WS, horizontal wind speed at 140 m; ω, vertical velocity; R, correlation coefficient; N, sample number. In (b), the blue line is the 1:1 line, while the red line is the line of best fit.

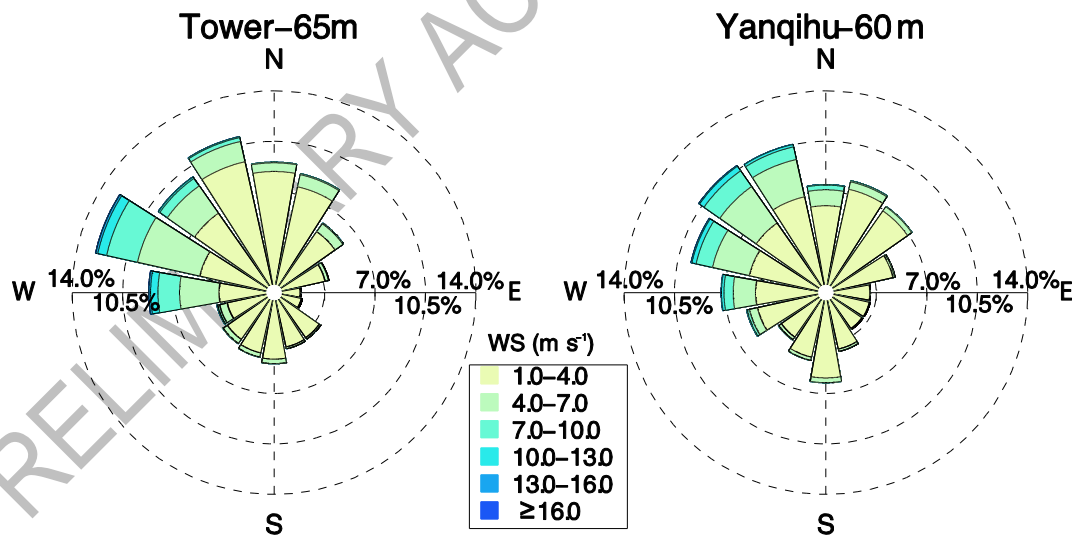

Fig. 3. Wind rose plots at 65 m AGL at the urban site (tower) and 60 m AGL at the suburban site (Yanqihu) based on observations from 22 October 2014 to 18 January 2015. The data at both sites were obtained every 20 s, with sample sizes of 383 810 and 356 075 at the tower and Yanqihu sites, respectively. The calm wind frequencies (< 1 m s^{-1}) were 12% at the tower site and 30% at the Yanqihu site. Notes: WS, horizontal wind speed.

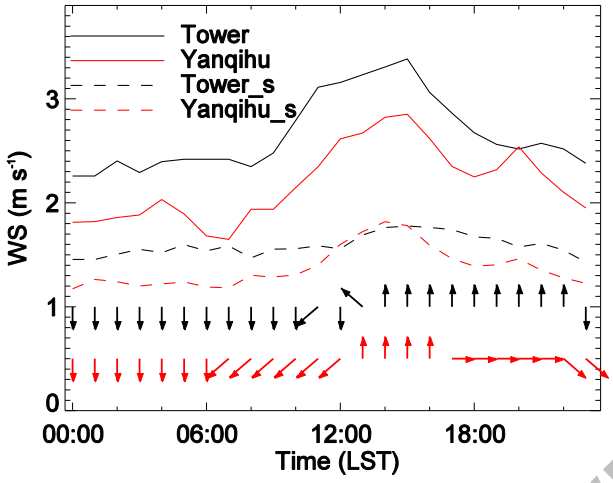

Fig. 4. Diurnal hourly wind speed (WS) and wind direction (highest frequency in eight directions) at 65 m AGL at the urban site (tower) and 60 m AGL at the suburban site (Yanqihu), based on observations from 22 October 2014 to 18 January 2015. WS is denoted by "_s" and wind direction is based on the WS data less than 3 m s^{-1}.

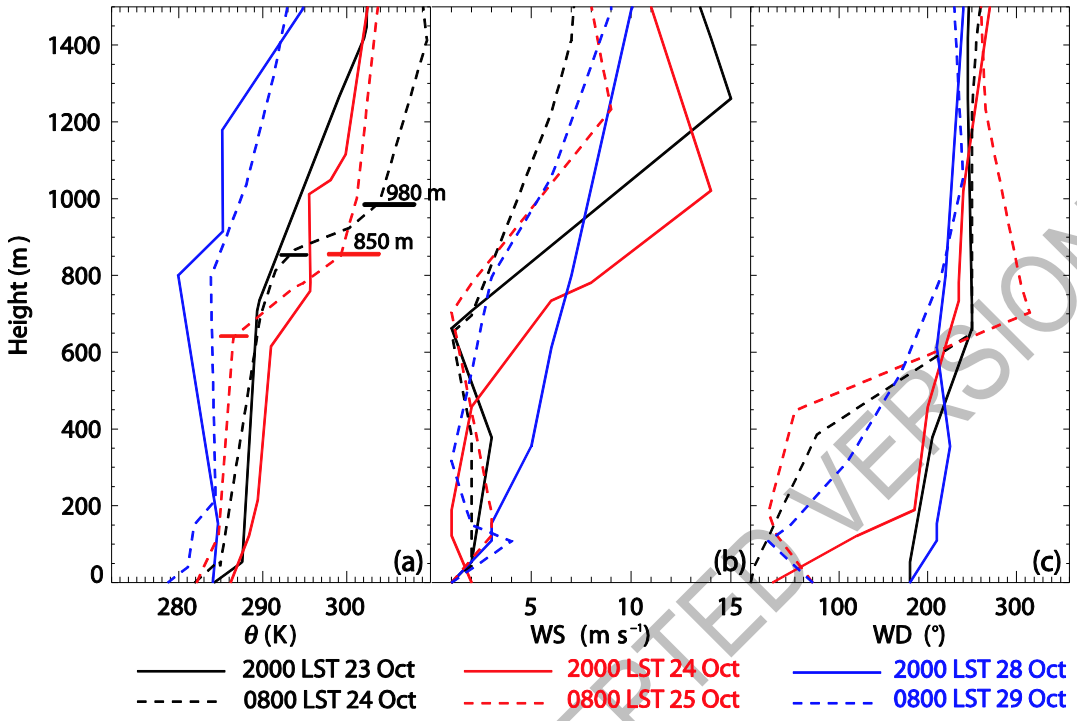

Fig. 5. Potential temperature (θ) and horizontal wind (WS, horizontal wind speed; WD, wind direction) profiles observed at the Nanjiao sounding site for the three events listed in Table 1. The temperature inversion layers at 0800 LST are marked by horizontal lines.

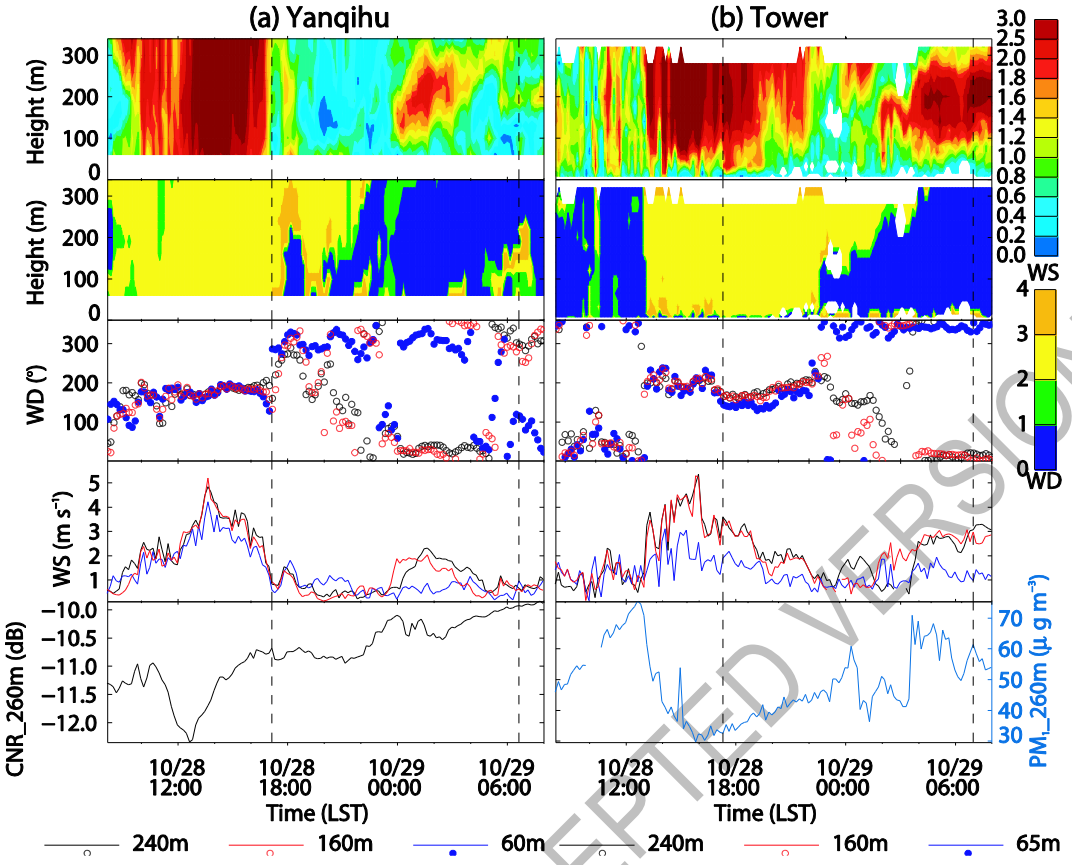

Fig. 6. Horizontal wind profiles, CNRs, and PM_1 mass concentrations observed at the Yanqihu and tower sites during 28 October 2014 (WS, horizontal wind speed; WD, wind direction, where a WD of 292.5°--360° and 0°--67.5° is represented by 0--1, and a WD of 112.5°--247.5° is represented by 2--3). The dashed lines mark the sunset and sunrise times.

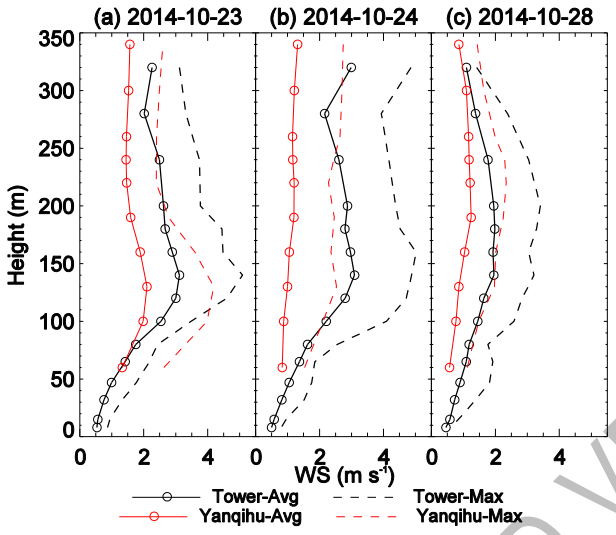

Fig. 7. Mean and maximum horizontal wind speed (WS; 10-min data) during 2300--0700 LST for the three events listed in Table 1.

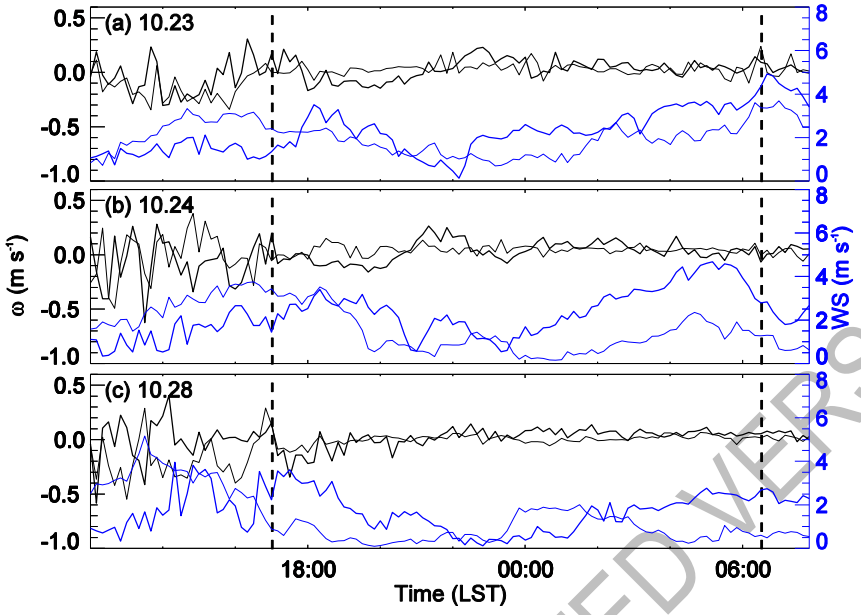

Fig. 8. The 10-min average vertical velocities (ω) and horizontal wind speeds measured at the Yanqihu site (the thin line represents results measured by the WLS8 at 160 m AGL) and the tower site (the thick line represents results measured by the sonic anemometer at 140 m AGL). The dashed line marks the sunset and sunrise times.

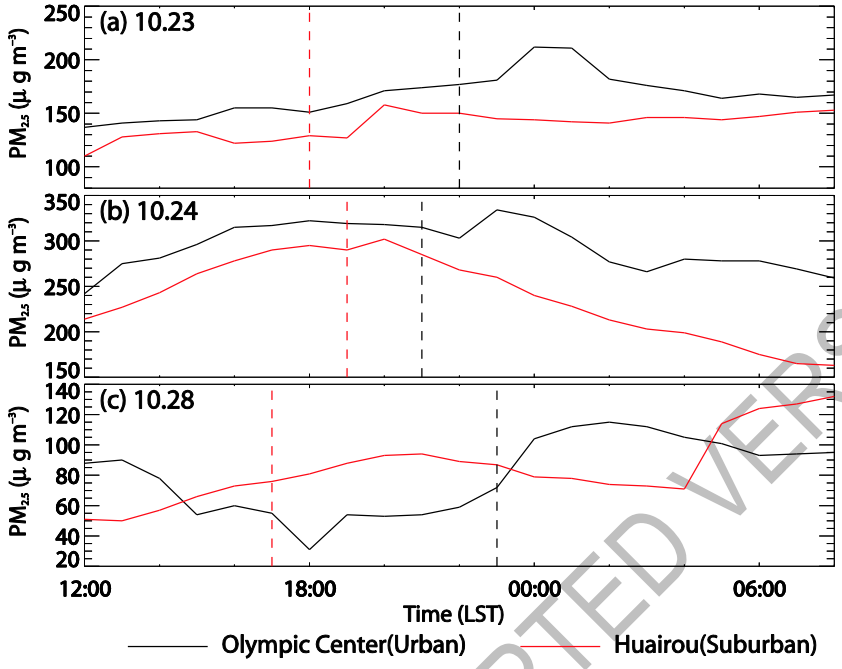

Fig. 9. One-hour surface $PM_{2.5}$ mass concentration observed at the Olympic Center (urban) and Huairou (suburban) sites. The dashed lines mark the wind direction shift times at the tower (black dashed line; 47 m AGL) and Yanqihu (red dashed line; 60 m AGL) sites, based on Table 1.

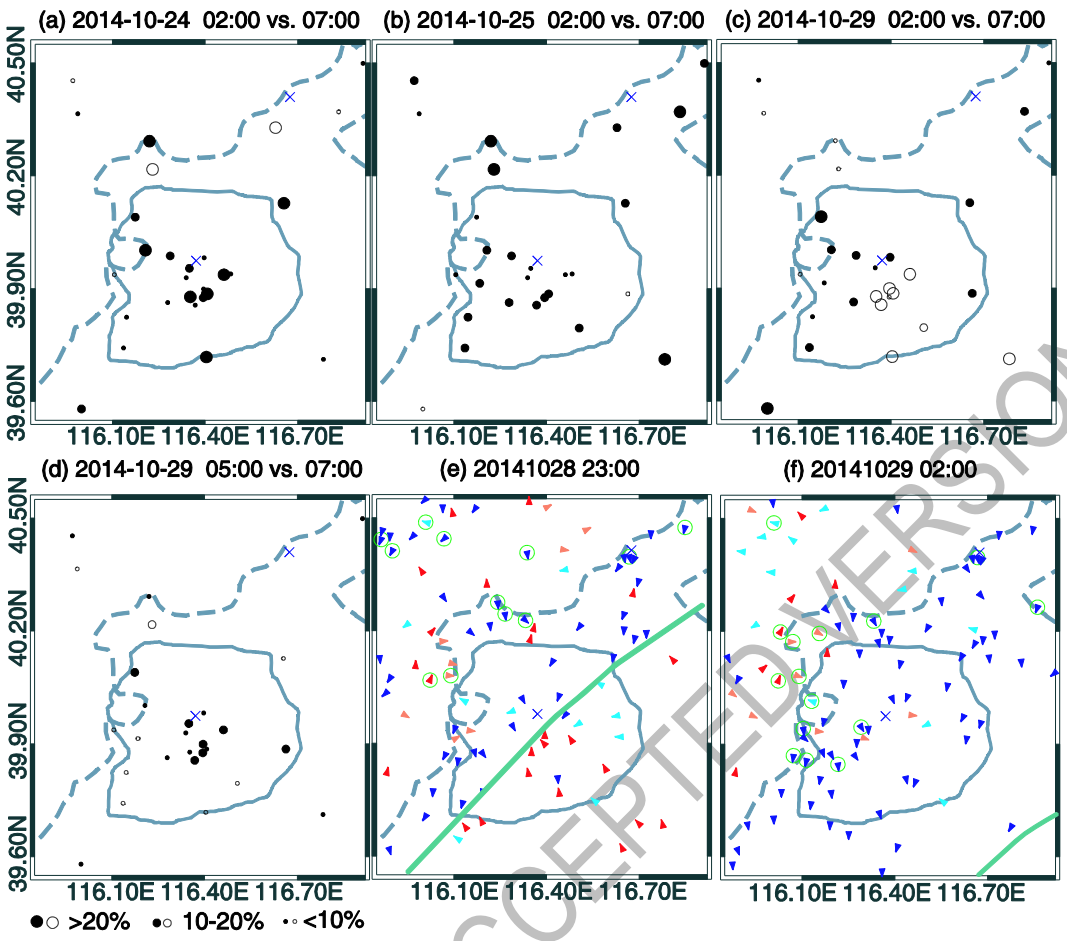

Fig. 10. (a--d) Relative variations in surface $PM_{2.5}$ mass concentrations, where filled circles represent a decrease in time and open circles represent an increase in time (LST) from (a) to (d); and (e, f) the horizontal distribution of 10-m wind measured by automatic weather stations. The dashed gray line indicates the 200-m topography line, while the solid gray line indicates the 6th ring road. The solid green line indicates the surface wind convergence line. The multiplication signs indicate the locations of the Yanqihu and tower sites. The green circle represents wind speeds greater than 1.5 m s^{-1}; dark blue wind vectors indicate northerly winds, and red indicates southerly winds.

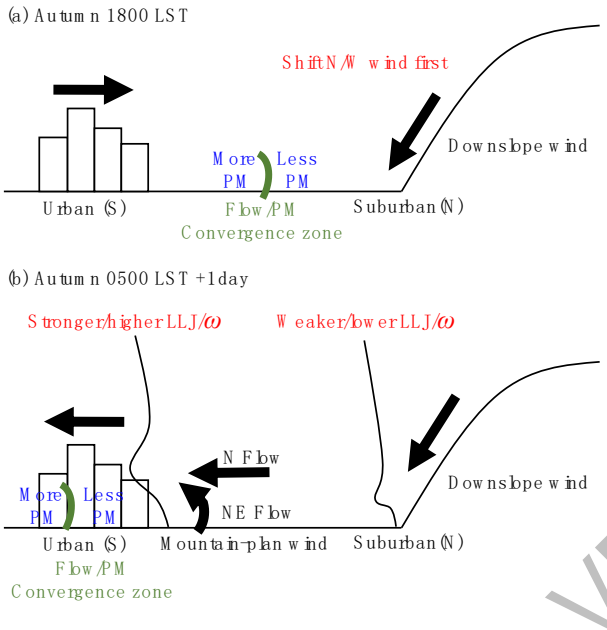

Fig. 11. Schematic illustration of nocturnal mountain breezes and their impacts on PM over Beijing at both suburban and urban sites.

Electronic Supplementary Material to: Nocturnal Low-level Winds and Their Impacts on Particulate Matter over the Beijing Area*

Yong CHEN[1], Junling AN[1,2,4], Yele SUN[1,2], Xiquan WANG[1], Yu QU[1], Jingwei ZHANG[1,2], Zifa WANG[1,2], and Jing DUAN[3]

[1]*State Key Laboratory of Atmospheric Boundary Layer Physics and Atmospheric Chemistry, Institute of Atmospheric Physics, Chinese Academy of Sciences, Beijing* 100029, *China*

[2]*College of Earth Science, University of the Chinese Academy of Sciences, Beijing* 100049, *China*

[3]*Chinese Academy of Meteorological Sciences, Beijing* 100081, *China*

[4]*Center for Excellence in Regional Atmospheric Environment, Institute of Urban Environment, Chinese Academy of Sciences, Xiamen* 361021, *China*

ESM to: Chen, Y., J. L. An, Y. L. Sun, X. Q. Wang, Y. Qu, J. W. Zhang, Z. F. Wang, and J. Duan, 2018: Nocturnal low-level winds and their impacts on particulate matter over the Beijing area. *Adv. Atmos. Sci.*, **35**(12), 000--000, https://doi.org/10.1007/s00376-018-8022-9.

* The online version of this article can be found at https://doi.org/10.1007/s00376-018-8022-9.

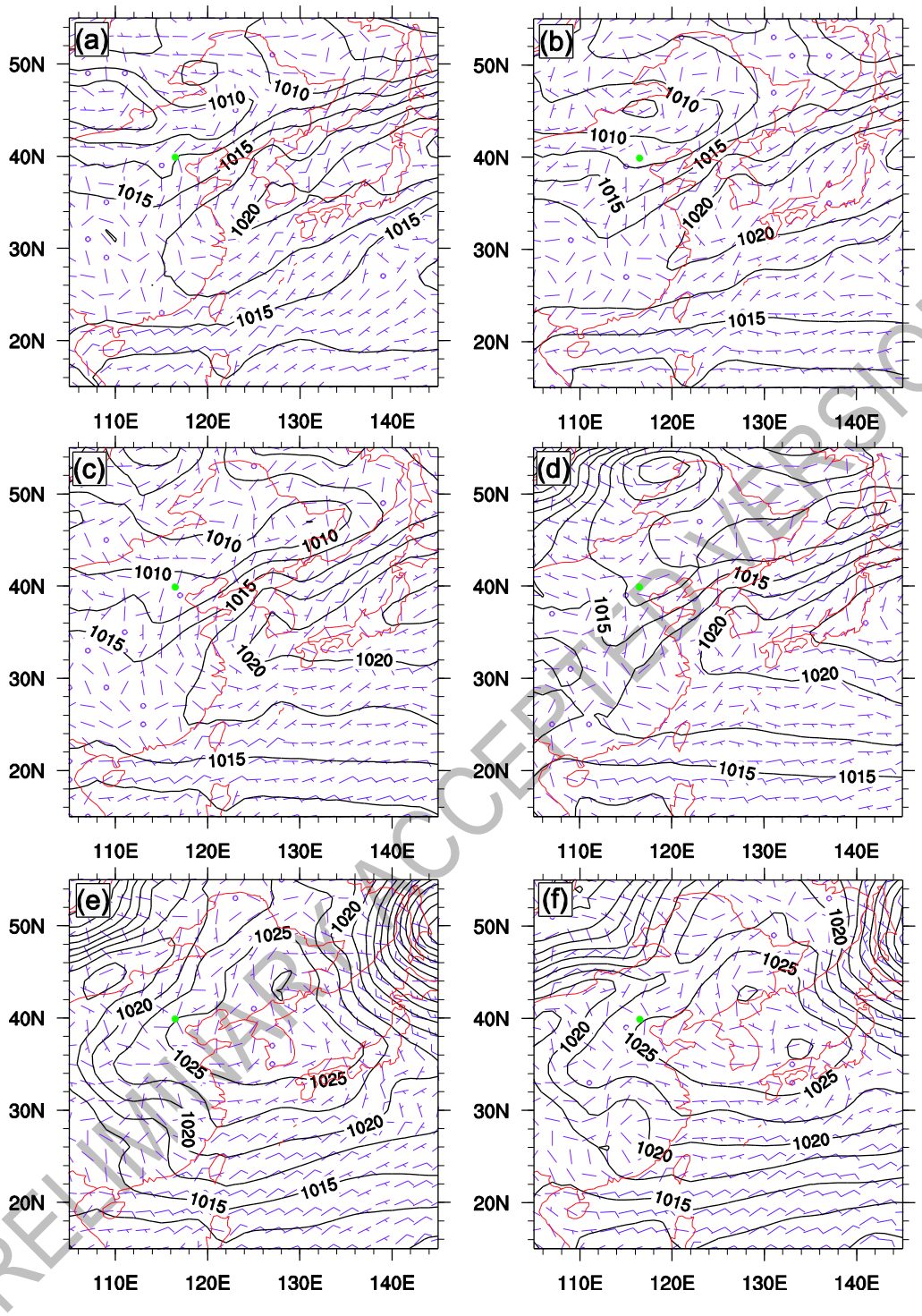

Fig. S1. Sea level pressure field (units: hPa) and 10-m wind field (unit: m s^{-1}) at (a) 2000 LST 23 October, (b) 0800 LST 24 October, (c) 2000 LST 24 October, (d) 0800 LST 25 October, (e) 2000 LST 28 October, and (f) 0800 LST 29 October, based on NCEP (1° × 1°) reanalysis data. The green dot denotes the location of Beijing.

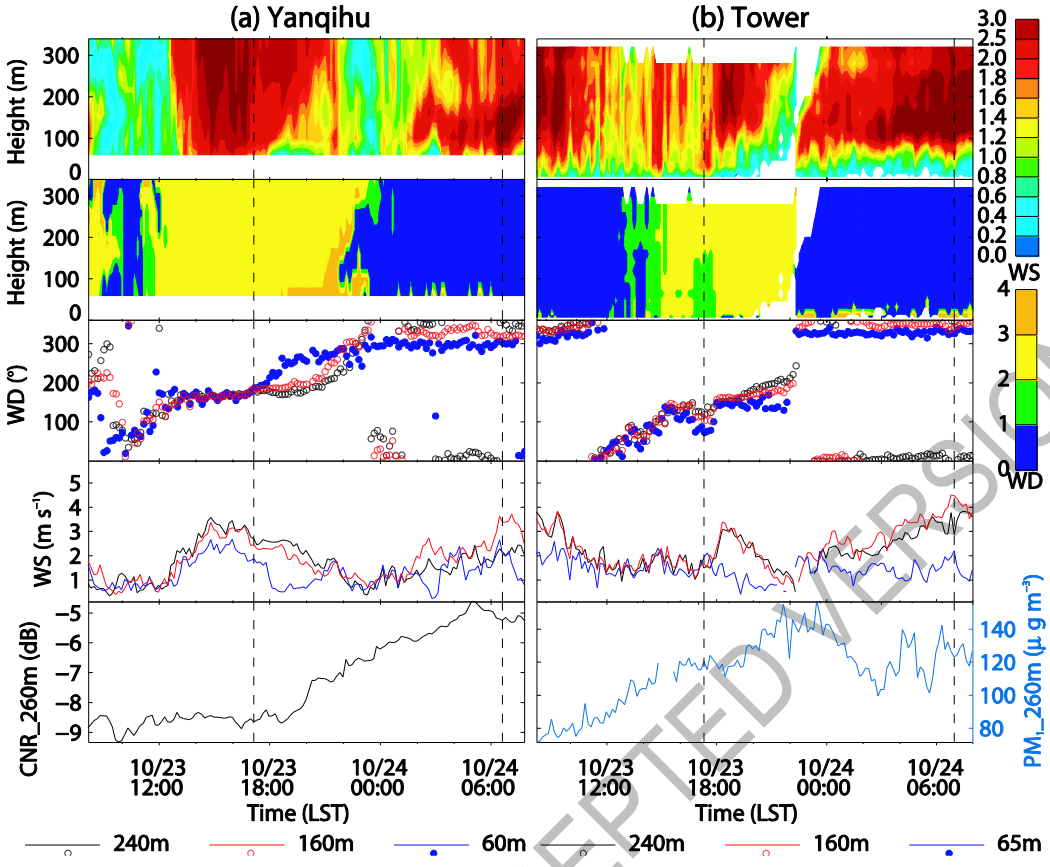

Fig. S2. Horizontal wind profiles, CNRs, and PM_1 mass concentrations observed at the Yanqihu and tower sites on 23 October 2014 (WS, horizontal wind speed; WD, wind direction, where a WD of 292.5°--360° and 0°--67.5° is represented by 0--1, and a WD of 112.5°--247.5° is represented by 2--3). The dashed lines mark the sunset and sunrise times.

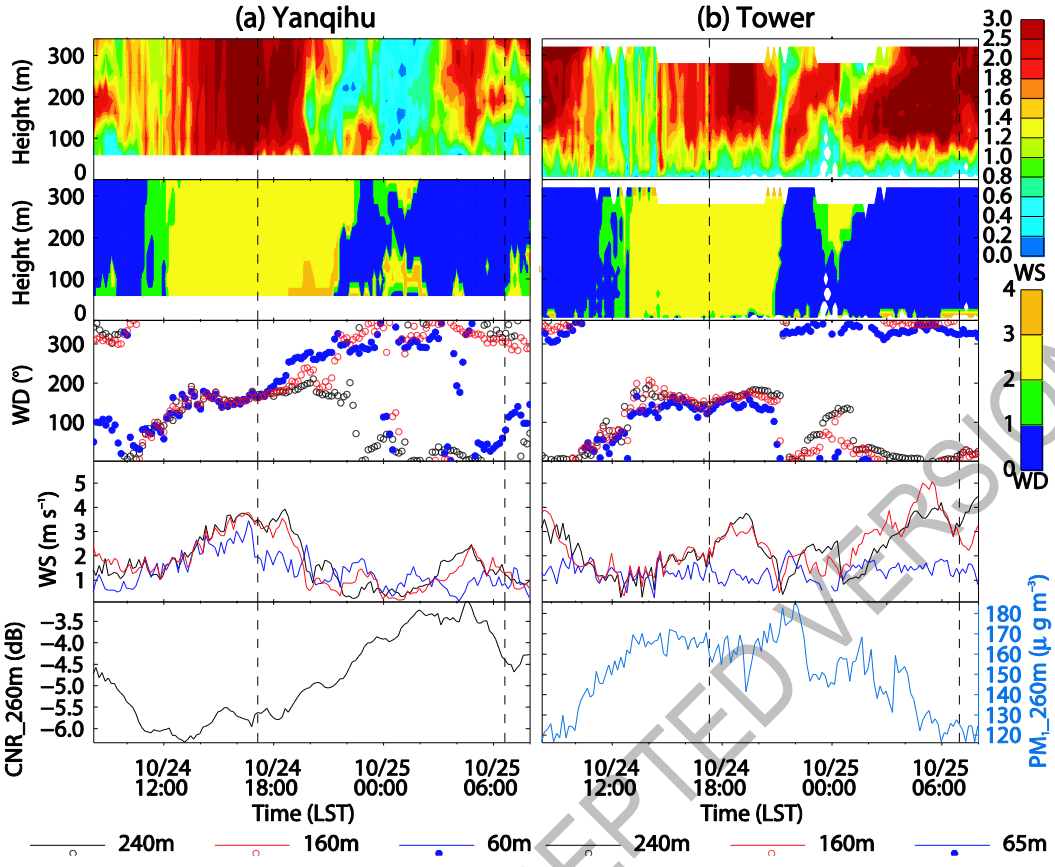

Fig. S3. Horizontal wind profiles, CNRs, and PM_1 mass concentrations observed at the Yanqihu and tower sites on 24 October 2014.

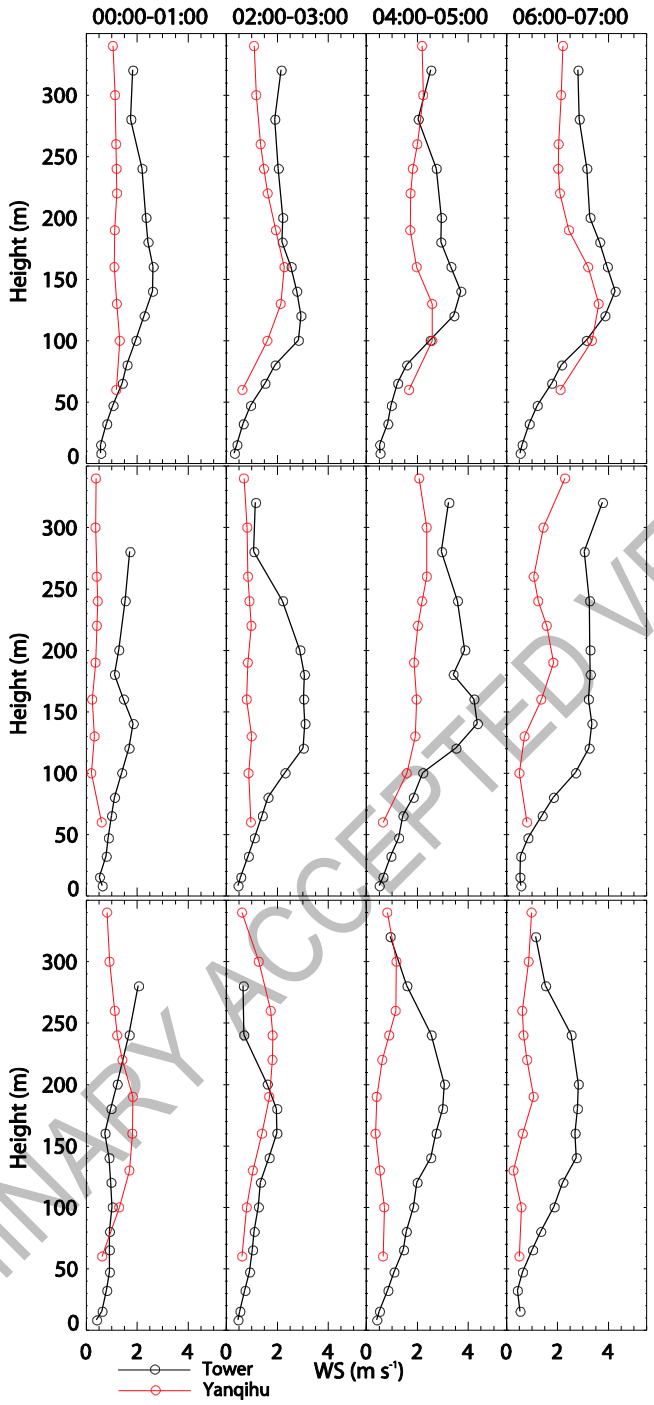

Fig. S4. Hourly mean wind speed (WS) profiles for three events on 23 (upper panel), 24 (middle panel) and 28 (lower panel) October 2014.